Acta Materialia 111 (2016) 31–38

Contents lists available at ScienceDirect

Acta Materialia

journal homepage: www.elsevier.com/locate/actamat

Full length article

A direct comparison of high temperature nanoindentation creep and uniaxial creep measurements for commercial purity aluminum

P. Sudharshan Phani*, W.C. Oliver

Nanomechanics Inc., 105 Meco Ln, Oak Ridge, TN, 37830, USA

ARTICLE INFO

Article history:
Received 14 October 2015
Received in revised form
9 March 2016
Accepted 10 March 2016
Available online 25 March 2016

Keywords:
Aluminium alloy
Creep
High temperature deformation
In situ
Nanoindentation

ABSTRACT

Measuring the uniaxial creep response from nanoindentation has been of great interest to the small scale mechanics community. However, several experimental and modeling challenges pose obstacles to direct comparison of indentation and uniaxial results. In this work, new experimental procedures are developed to improve the precision and accuracy of high temperature nanoindentation tests. Indentation creep experiments are performed on commercial purity aluminum alloy at a number of temperatures up to 550 °C. The activation energy for creep was found to be 140.2KJ/mol/K, matching the value determined with high temperature uniaxial creep experiments extremely well. Uniaxial power-law creep parameters (stress exponent and pre-exponential term) are calculated from the indentation data for direct comparison of results to the uniaxial data. The results are in good agreement with the literature values for uniaxial compression/torsion tests over a wide range of strain rates and temperatures demonstrating the capabilities of high temperature indentation creep experiments. The relative contributions and interplay of indentation size effect, strain rate and temperature on the creep response is also explored.

1. Introduction

Recently, there has been an increased interest in high temperature nanoindentation due to improved instrumentation and better experimental techniques [1–7]. This has further extended the capability of nanoindentation based techniques to study temperature and rate effects on the mechanical properties of small volumes of materials. In this regard, there is great value in measuring the uniaxial creep response from indentation especially with the commonly used Berkovich indenter. However, the complexity of stress fields during indentation often precludes direct measurement of uniaxial constitutive behavior [8]. For instance, in the case of power-law creep, it is relatively simple to measure the uniaxial stress exponents [9] from indentation but not the uniaxial pre-exponential terms. However, Su et al. [8] recently proposed a simple experimental technique to measure the uniaxial power-law creep parameters (stress exponent and pre-exponential term) by instrumented indentation based on a theoretical analysis of Bower et al. [10] and showed good agreement between the indentation and uniaxial results for amorphous selenium at 35 °C. However, the technique has not been validated on more commonly used engineering materials at high temperatures.

Performing nanoindentation measurements at elevated temperatures is challenging on several fronts as elucidated elsewhere [3,7]. These challenges limit the use of the experimental data especially for studying creep at elevated temperatures. In this work, we present new experimental techniques to address some of these challenges and improve the accuracy and precision of the measurements at elevated temperatures. Indentation creep experiments are performed on the widely used commercial purity aluminum alloy (1100 Al) alloy at a number of temperatures up to 550 °C to measure the uniaxial power-law creep parameters (stress exponent and pre-exponential term). These results are compared to the uniaxial compression/torsion data to assess the feasibility of measuring uniaxial power-law creep parameters using high temperature nanoindentation. Recently, several research groups have also explored the temperature dependence of size effects and the interplay between size effects and rate effects [11–15]. Here, we present the relative effects of temperature, strain rate, indentation size effect (ISE) and microstructure on the measured creep response to identify the best experimental procedures to study indentation creep at elevated temperatures.

* Corresponding author.
E-mail address: s.phani@nanomechanicsinc.com (P.S. Phani).

http://dx.doi.org/10.1016/j.actamat.2016.03.032
1359-6454/

2. Experimental procedures

2.1. Challenges and solutions

As mentioned earlier, performing nanoindentation measurements at elevated temperatures is challenging on several fronts. Here, we discuss the major challenges specific to indentation creep testing. While some of the issues cannot be completely addressed, we can significantly improve the precision and accuracy of the indentation creep measurements by the following guidelines.

2.1.1. Thermal equilibrium during testing

Maintaining thermal equilibrium between the tip and the sample during testing is very important [4]. However, engineering difficulties in precisely positioning the thermocouples and the associated thermal gradients due to the sample geometry are some of the obstacles to achieving this. To overcome this issue, we use a simple procedure assuming that if the tip and the sample are in thermal equilibrium, the temperature of the tip does not change upon contact with the sample. The tip temperature is initially set to the desired value and contact is established with the sample. The sample temperature (close to the tip temperature) that does not result in any change in tip temperature upon contact with the sample is then determined. Note that, it is still important to have a thermally stable testing system and to position the thermocouples as close to the region of interest as possible to minimize this offset. Fig. 1 shows the change in tip temperature upon contact with the sample at different temperatures, while the tip is nominally being maintained at 250 °C. It is evident from the plot that the sample temperature can be adjusted to minimize the change in the tip temperature upon contact. In this case, a sample temperature of 268.3 °C results in virtually no change in tip temperature upon contact, thereby resulting in thermal equilibrium during testing. This procedure can be repeated once at every test temperature for a given sample to determine the offset. Fig. 2 shows the tip temperature upon contact with the sample at different set temperatures after determining the respective offsets. For a wide range of test temperatures shown in the plot, there is no significant change in the tip temperature upon contact thus ensuring thermal equilibrium during mechanical testing. The offset between the tip and sample temperatures results is some ambiguity in accurately determining the test temperature. However, as the tip thermocouple is closest to the contact, the tip temperature is taken to be the test temperature in this work.

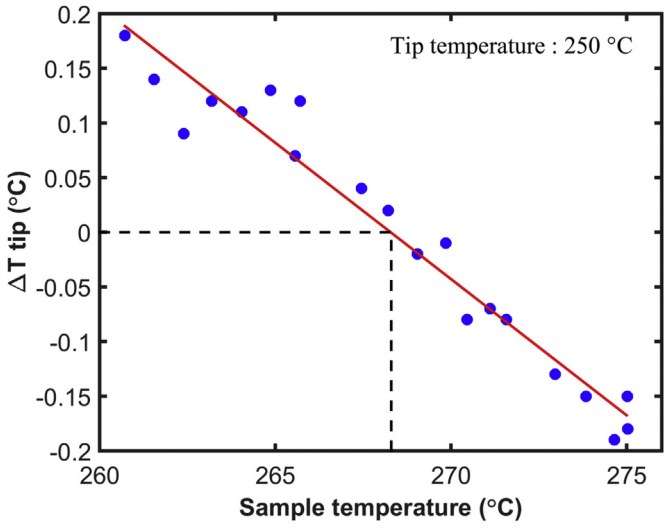

Fig. 1. Change in tip temperature upon contact with the sample at different temperatures. In this case, the tip temperature is maintained at 250 °C.

2.1.2. Thermal drift

Thermal drift is the displacement that results from the dimensional changes caused due to the thermal fluctuations within the testing system. It is one of the major factors that affect nanoindentation measurements especially at elevated temperatures. Performing fast tests while maintaining low drift rates and properly accounting for the thermal drift can help overcome drift issues. This is even more critical for creep testing where the test duration is much longer than usual. Here we describe a simple procedure to determine the thermal drift during high temperature nanoindentation testing where traditional methods to correct for drift cannot be used.

The procedure relies on the fact that in a well-designed high temperature nanoindentation system, thermal drift can be directly correlated to the temperature changes of the tip and the sample. The procedure involves systematically varying the tip and the sample temperatures to result in displacement changes that can be completely attributed to thermal drift. A simple model can then be used to correct the displacement using the known temperature variations. The following equation is used to correct the displacement for static and dynamic variations in tip and sample temperatures.

$$h_{corr}(t) = h(t) + \alpha\Delta T_{tip}(t+\tau_{tip}) + \beta\Delta T_{sample}\left(t+\tau_{sample}\right), \qquad (1)$$

where, h_{corr} is the drift corrected displacement, h is the uncorrected displacement, α and β are the tip and sample temperature coefficients respectively and τ_{tip} and τ_{tip} are akin to the thermal time constants of the tip and the sample. Fig. 3a shows the temperature fluctuations purposely and systematically induced on the tip and sample. Large variations in temperatures have been deliberating introduced to improve the accuracy of the model. However, the typical temperature variation during a creep test is <0.05 °C. Fig. 3b shows the uncorrected and temperature corrected displacement using Eq. (1). The fact that the corrected displacement is almost zero for any type of temperature variation indicates that the current experimental setup can be precisely modeled by Eq. (1), thereby enabling high temperature measurements without any significant drift. Note that, it is still important to have a thermally stable testing system with small changes in displacement for a given temperature change.

2.1.3. Indentation size effect (ISE)

ISE commonly refers to a phenomenon where the hardness changes as a function of probed volume or impression size [16]. This can lead to misinterpretation of indentation creep data where the desire is to measure strain rate effects directly. This issue can be addressed by performing creep tests at large depths, where the ISE is not only less significant but also the additional creep displacements do not change the contact area as much as at shallower depths. Large indents also minimize the errors due to tip area calibration.

2.1.4. Inhomogeneous sample

Most engineering materials are usually not homogeneous at small length scales and hence can exhibit local variations in mechanical properties at that scale. For example, commercial purity aluminum (1100 Al) has less than 1% of many minor phases of Fe-Al-Si that alter the local mechanical properties. This can lead to inaccuracies in the creep data especially if hardness at different strain rates is measured at different locations. This can be partly addressed by measuring hardness over a wide range of strain rates at the same location. Additionally, performing a large number of tests can provide better statistics for samples with

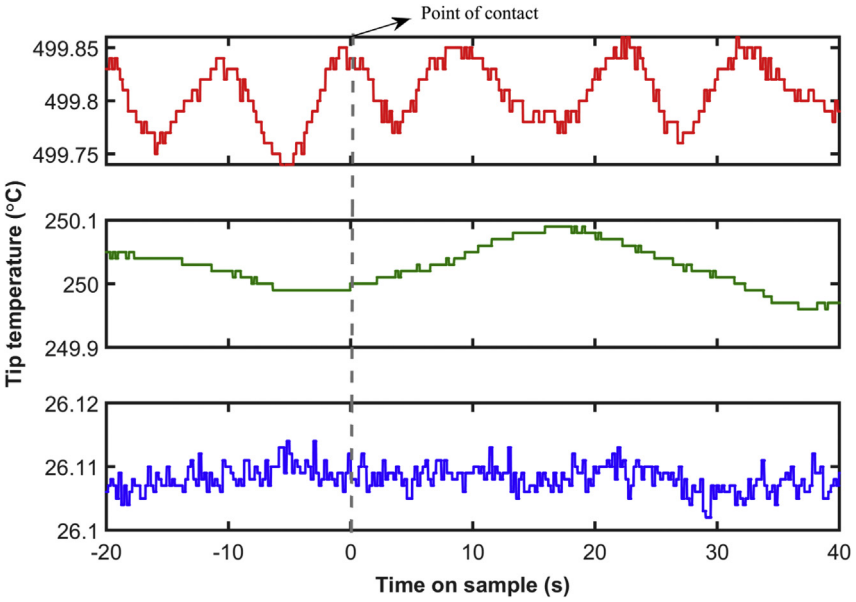

Fig. 2. Tip temperature upon contact with the sample at different set temperatures. The tip contacts the sample surface at a time on sample of 0 s.

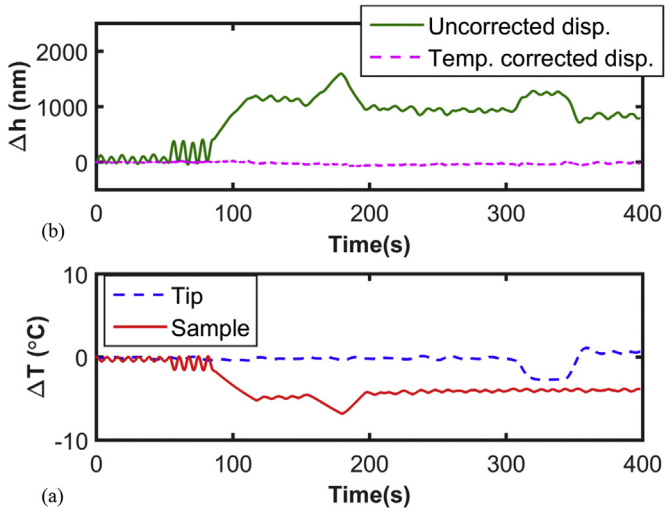

Fig. 3. (a) Systematically induced tip and sample time-temperature history. (b) Uncorrected and temperature corrected displacement as a function of time for the systematically induced tip and sample temperature variations.

inhomogeneities. This is practical if the test durations are short, which also helps minimize drift correction and improves the repeatability of the results.

The most common types of indentation creep tests using a Berkovich indenter are constant load and hold (CLH) [17], constant rate of loading (CRL) [18], constant strain rate (CSR) [19] and strain rate jump tests [19]. While the CSR test enables testing at a fixed strain rate where the microstructure might be more akin to steady state, the CLH, CRL and strain rate jump tests enable access to multiple strain rates in a single test (or location) and thereby improve the precision of the measurements across a range of strain rates. The range of depths required to measure the relationship between strain rate and strength with a CLH test is typically smaller than the CSR, CRL and strain rate jump test, thus making it less susceptible to the effects of an ISE.

In light of the above discussion, one possible simple test procedure that addresses the major issues is the constant load and hold or CLH test. This involves fast loading to a prescribed load to generate a large contact and maintaining a constant load or force for a short duration to measure the resultant creep displacement. This not only minimizes the ISE and drift issues but also enables hardness measurements at multiple strain rates at the same location. Note that CLH tests may not be the best option if effective steady state conditions cannot be reached while a constant load is being maintained or if the microstructure evolution has history dependence.

2.2. Testing equipment and testing conditions

Indentation creep measurements were performed inside an scanning electron microscope using an InSEM HT (Nanomechanics Inc., Oak Ridge, TN), which is an in situ high temperature nanomechanical tester. It has an independent tip and sample heating system that is designed to maintain the temperature within ±0.05 °C. A Berkovich sapphire indenter tip was used instead of a diamond tip to perform tests at higher temperatures because of the possible degradation of the diamond indenter due to graphitization or chemical reaction with the sample.

Constant load and hold (CLH) indentation creep tests were performed at several temperatures ranging from room temperature to 550 °C (27 °C, 50 °C, 98 °C, 147 °C, 193 °C, 250 °C, 292 °C, 382 °C, 430 °C, 500 °C and 550 °C). All the tests were performed on a 10 mm diameter commercial purity aluminum (1100 aluminum) sample which was polished and subsequently annealed at 350 °C for 4 h before testing. At least 5 repetitive tests were performed at each temperature to ensure repeatability in the data. The CLH tests were performed by ramping the load to 16 mN in 1 s and subsequently maintaining a constant force for 40 s. Additionally, constant strain rate tests at strain rates of 0.1 s^{-1} and 0.5 $s^{-1}$and strain rate jump tests [19,20] from 0.1 s^{-1} to 0.5 s^{-1} were performed at room temperature and 400 °C. For these tests, the contact stiffness was continuously measured as a function of depth using a phase lock amplifier oscillating at 100 Hz.

3. Calculation of uniaxial power-law creep parameters

The theoretical analysis proposed by Bower et al. [10] and the

experimental method proposed by Su et al. [8] forms the basis for calculating the uniaxial power-law creep parameters from indentation data. The final expressions used to calculate the uniaxial power-law–creep parameters are presented here while the details can be found in Su et al. [8]. The mathematical equation for power-law creep relating the steady state strain rate ($\dot{\varepsilon}$) and stress (σ) for a uniaxial creep test can be written as

$$\dot{\varepsilon} = A\sigma^n, \tag{2}$$

where n is the uniaxial stress exponent and A is the uniaxial pre-exponential term. Similar power-law creep equation for indentation strain rate ($\dot{\varepsilon}_i$) takes the form [8].

$$\dot{\varepsilon}_i = \left(\frac{1}{h}\right)\left(\frac{dh}{dt}\right) = B(p_{nom})^N = B\left(\frac{L}{\pi(h\tan\theta)^2}\right)^N, \tag{3}$$

where h is the indentation depth, L is the load, N is the indentation stress exponent, B is the indentation pre-exponential term and p_{nom} is the nominal contact pressure calculated from the load and the projected area corresponding to the indentation depth.

Note that under effective steady state conditions, the stress exponent is identical for uniaxial and indentation testing (i.e., $N = n$) [8] and henceforth will be referred to as stress exponent (n) for both indentation and uniaxial tests. The uniaxial pre-exponential term (A) can be calculated from the indentation data using the following equation [8],

$$A = \frac{BF^n c^{2n-1}}{\tan\theta}, \tag{4}$$

where, θ is the equivalent half cone angle, c is the pile-up/sink-in parameter and F is the reduced contact pressure. F and c are functions of stress exponent and cone angle and their functional dependence has been determined by finite element analysis (equations (10) and (11) along with fit parameters in Tables 1 and 2 of Su et al. [8]). Finally, the equivalent uniaxial strain rate and stress can be calculated from the basic indentation measurements (h and L) using the following equations.

$$\dot{\varepsilon} = \left(\frac{1}{c\tan\theta}\right)\left(\frac{1}{h}\right)\left(\frac{dh}{dt}\right). \tag{5}$$

$$\sigma = \left(\frac{1}{Fc^2}\right)\left[\frac{L}{\pi(h\tan\theta)^2}\right]. \tag{6}$$

In this work, we first determine the stress exponent (n) from the slope of the $log(\dot{\varepsilon}_i)$ versus $log(p_{nom})$ or $log(Hardness)$ and subsequently calculate the pile-up/sink-in parameter (c) and the reduced contact pressure (F) from the stress exponents using the equations given in Su et al. [8]. Finally, we calculate the equivalent uniaxial strain rate ($\dot{\varepsilon}$) and stress (σ) using equations (5) and (6).

4. Results and discussion

4.1. Constant load and hold tests: basic measurements

Fig. 4 shows the indentation depth as a function of time on sample for the CLH tests at all the test temperatures. The plot shows two distinct regions: the fast initial increase in depth corresponding to the fast load ramp (16 mN/s) and the subsequent creep at a fixed force of 16 mN. The maximum depth reached during each test and the creep rate increases with temperature as expected. Note that at low temperatures (27 °C and 50 °C) the creep rates are

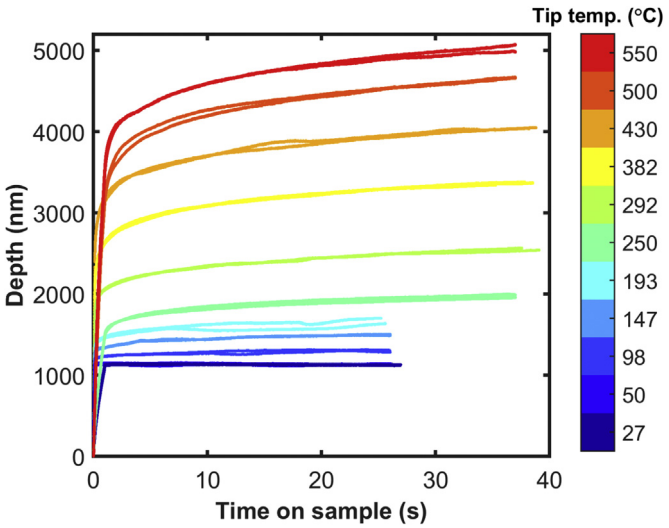

Fig. 4. Depth as a function of time for CLH tests at different temperatures.

almost insignificant. While this may be expected for aluminum, it has implications for achieving steady state which will be discussed later. In order to calculate hardness from this data, the contact area needs to be estimated. This is done by assuming a constant ratio of contact depth to the total depth which can be calculated from the unloading data at the end of each test. This ratio is around 0.99 for all the tests and hence the contact depth is almost equal to the total depth for all the tests. Fig. 5 shows the hardness as a function of indentation depth during loading at all the temperatures. Note that Fig. 5 only shows hardness during the initial load ramp and not during the hold segment. From the plot it is clear that this sample exhibits ISE. However, major portion of the size effect is exhausted by the end of loading, demonstrating one of the relative merits of indentation creep measurements using CLH tests to large depths.

4.2. Temperature and strain rate effects

In this section, we analyze the effect of strain rate and temperature on the hardness for the CLH tests. Fig. 6 shows a log–log plot of indentation strain rate as a function of hardness during the hold period of the CLH tests at all the test temperatures. The indentation

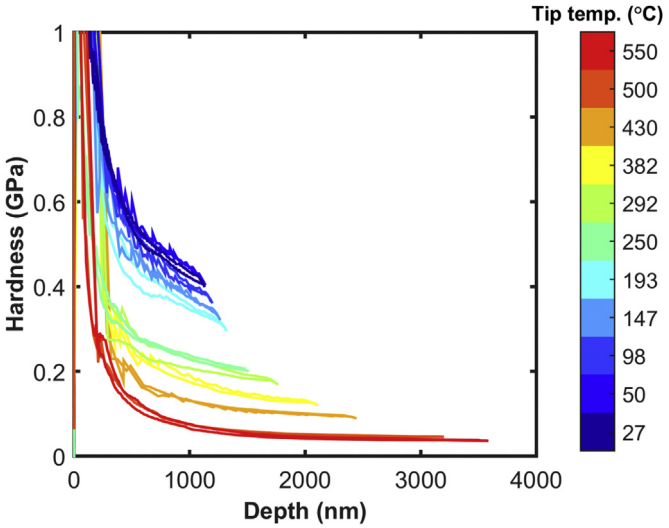

Fig. 5. Hardness as a function of depth during loading for CLH tests at different temperatures.

strain rate is the ratio of indenter velocity ($\dot{h}$) to the depth (h) as shown in Eq. (3). The plot shows a fairly linear relationship between indentation strain rate and hardness across four orders of magnitude in strain rate. The stress exponents at various temperatures can be measured from the slope of this plot. The plot also shows the increase in slope with decreasing temperature as expected. Interestingly, the room temperature data has a near vertical slope and the possible reasons for that will be discussed later.

Creep at high temperatures for aluminum is known to exhibit an Arrhenius type behavior and the strain rate at a constant stress can be written as

$$\dot{\varepsilon} = \dot{\varepsilon_o} exp\left(-\frac{Q}{RT}\right), \tag{7}$$

where, $\dot{\varepsilon_o}$ is a constant, Q is the apparent activation energy for creep, R is the universal gas constant and T is the absolute temperature. The apparent activation energy can thus be calculated from the slope of natural logarithm of indentation strain rate plotted versus $1/T$. Fig. 7 shows the Arrhenius plot at a constant hardness (equivalent to constant stress) of 0.1 GPa for homologous temperatures above 0.6. The apparent activation energy calculated from the slope is 142.4 kJ/mol/K which compares well with a value of 142 kJ/mol/K reported in literature for this temperature range [21].

In order to compare the strain rate dependence of hardness across multiple temperatures, the strain rate and hardness need to be compensated for diffusion at the test temperature. While a more rigorous approach will be presented in the next section, here we simply normalize the strain rate by $exp(-\frac{Q}{RT})$ and the hardness by the temperature dependent Young's modulus (E) [22] to enable comparison of creep data across different temperatures. While activation energy is calculated as discussed earlier, the temperature dependent Young's modulus is taken from Lucas [19]. Fig. 8 shows a log–log plot of temperature compensated indentation strain rate versus ratio of hardness to the Young's modulus for all the test temperatures. The indentation creep data from all the temperatures collapses onto a single curve indicating that the deformation is controlled by a single thermally active process without any apparent history dependence. This result also demonstrates the ability to perform reliable creep measurements over a wide range

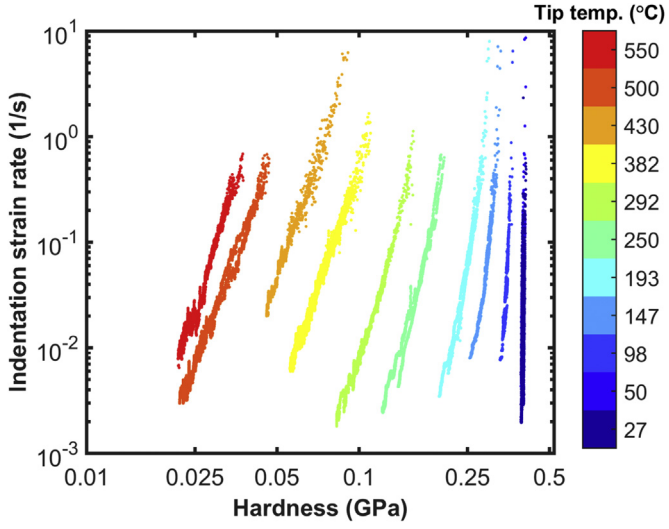

Fig. 6. Log–log plot of indentation strain rate as a function of hardness for CLH tests at different temperatures.

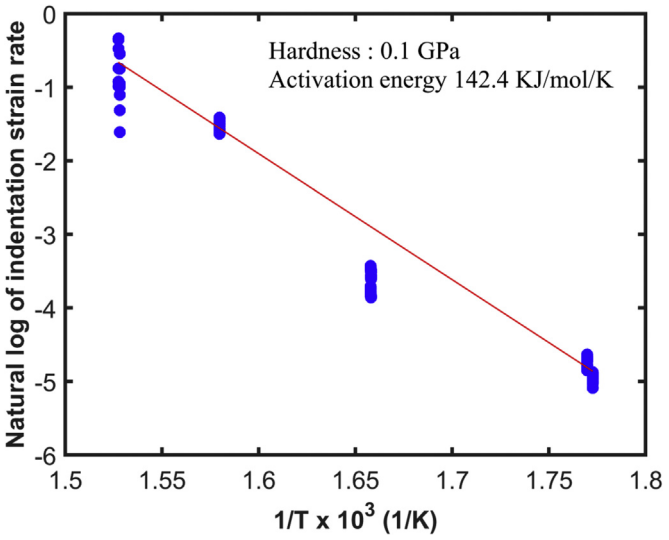

Fig. 7. Natural logarithm of the indentation strain rate as a function of reciprocal of the absolute temperature at a constant hardness value of 0.1 GPa. The apparent activation energy for creep calculated from the slope is also shown.

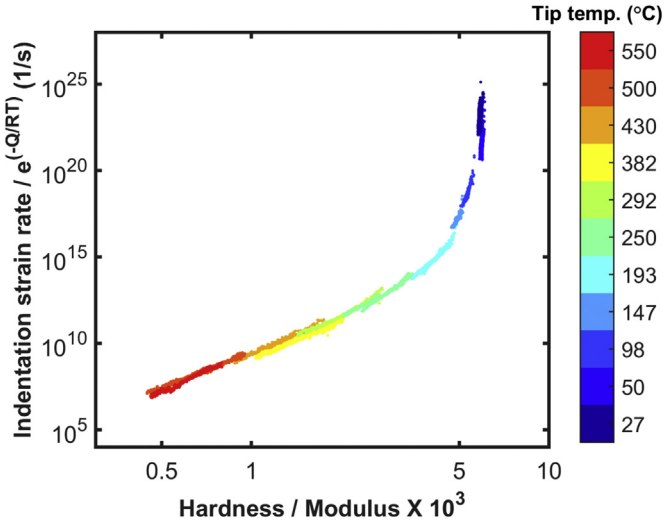

Fig. 8. Temperature compensated indentation strain rate as a function of normalized hardness for CLH tests at different temperatures.

of temperatures without being limited by the experimental challenges discussed in section 2.1. It is interesting to note that the plot shows a largely linear region followed by a region that curls up to a higher slope at the lower temperatures. This could be due to the inability to achieve a steady state microstructure at the lower temperatures which will be discussed in detail in the next section.

4.3. Estimating the uniaxial power-law creep parameters

In this section, we present the equivalent uniaxial strain rate and stress calculated from the indentation creep data, which is then compared with the uniaxial data from the literature. The uniaxial equivalent strain rate and stress can be calculated using the method proposed by Su et al. [8] as shown in Eq. (5) and Eq. (6) respectively. The parameters F and c required in these calculations are unique functions of the stress exponents for a given cone angle and are calculated from the equations given in Su et al. [8]. It is interesting

to note that for the stress exponents observed in this work (>5), the parameter F is almost a constant (~2.71). The uniaxial data thus calculated can be compared across different temperatures by calculating the temperature compensated strain rate and the modulus compensated hardness as indicated by Luthy et al. [21]. They showed that under steady state conditions, the strain rate and stress are related by the following functional form,

$$\frac{\dot{\varepsilon}}{D_{eff}} = f\left(\frac{\sigma}{E}\right). \tag{8}$$

where, D_{eff} is the effective diffusion coefficient. The effective diffusion coefficient as defined by Luthy et al. [21], takes into consideration two different lattice self-diffusion coefficients corresponding to different temperatures and dislocation pipe diffusion, which, for aluminum (in S.I. units) is given by

$$D_{eff} = 1.7 \times 10^{-4} exp\left(-\frac{142}{RT}\right) + 6 \times 10^{-7} exp\left(-\frac{115}{RT}\right) + 2.8 \times 10^{-6} exp\left(-\frac{82}{RT}\right)\left[80\left(\frac{\sigma}{E}\right)^2\right]. \tag{9}$$

Fig. 9 shows the temperature compensated uniaxial equivalent strain rate and the modulus compensated hardness at all the temperatures. Similar to the results observed by Luthy et al. [21] for uniaxial creep tests on pure aluminum, data from all the temperatures lie on a single curve, demonstrating the validity of the functional form of strain rate versus stress (Eq. (8)) for indentation creep. Given the vast differences in test geometries and test protocols between the uniaxial and indentation creep tests, it is interesting to note that the indentation creep data behaves very similar to the uniaxial data over 15 orders of magnitude in temperature compensated strain rate. While Fig. 9 demonstrates the good qualitative agreement in the functional dependence between the uniaxial and indentation data, it is instructive to directly compare the results to the uniaxial creep data on 1100 aluminum.

Fig. 10 shows a comparison of the temperature compensated strain rate as a function of modulus compensated hardness for indentation creep and uniaxial tests [23]. Uniaxial results at two different strains (10% and 70%) are shown for comparison. The uniaxial results were obtained by inspecting the literature results for multiple constant strain rate tests at several temperatures and subsequently analyzing the results at a fixed value of strain. Excellent agreement over 10 orders of magnitude in temperature compensated strain rate can be seen between the indentation data and the uniaxial data at 10% strain. The stress exponent from indentation at the highest test temperature (550 °C) is 7.72 ± 0.24 and compares well with a value of 7.69 from the uniaxial data at 10% strain. However, the uniaxial data at 70% strain deviates towards higher modulus compensated hardness values, indicating that steady state conditions may not have been achieved in the uniaxial tests at 10% strain and the indentation tests in that region. This region corresponds to the low temperature tests (<100 °C) where the creep displacements are small. This can result in the microstructure not reaching steady state where the rate of hardening is balanced by the rate of recovery [24]. Alternatively, it is possible that different amounts of minimum strain is required to achieve steady state conditions at different temperatures and the minimum strain at lower temperatures may be greater than 10%. Given that a Berkovich indenter induces a characteristic strain of around 8% [25], it may not be possible to achieve effective steady state at the lower temperatures for aluminum at that strain. For instance, Luthy et al. [21] performed torsion tests to large strains (300%–1000%) in order to achieve steady state creep at lower temperatures in pure aluminum. Fig. 11 shows a comparison of the indentation creep data on 1100 Al presented in this work with the steady state uniaxial tension/torsion data on pure aluminum from Luthy et al. [21]. While the two data sets show good agreement at the intermediate temperatures, some deviations can be seen at the higher and lower temperatures. At the higher temperatures, data from 1100 Al is steeper possibly due to the presence of Fe-Al-Si based precipitates that can result in higher stress exponents. Also, the indentation results may not be at effective steady state. At the lower temperatures, the indentation results show a sharp increase in slope while the uniaxial data has a smoother trend. As the uniaxial data at these temperatures was obtained from torsion experiments to large strains (300%–1000%) in order to reach steady state, it may be concluded that the indentation tests which are nominally at 8% strain do not correspond to an effective steady state. This also explains the difference in the uniaxial results at higher values of σ/E (lower temperatures) on 1100 Al at 10% and 70% strain.

As the present study covers a wide range of strain rates and

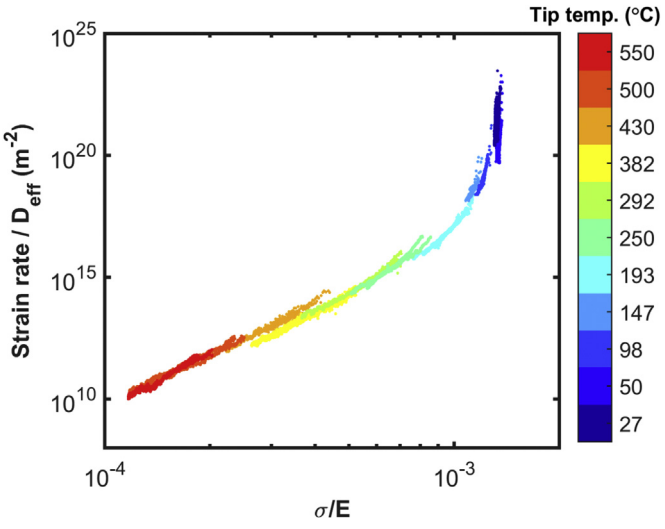

Fig. 9. Temperature compensated uniaxial strain rate as a function of normalized uniaxial stress for CLH tests at different temperatures.

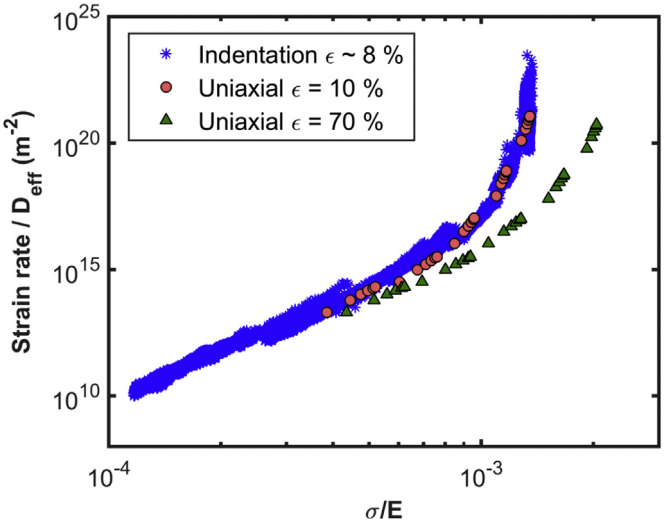

Fig. 10. Temperature compensated uniaxial strain rate as a function of normalized uniaxial stress. The plot shows the results from indentation creep experiments using a Berkovich indenter (~8% strain) and uniaxial experiments at a constant strain of 10% and 70% [23].

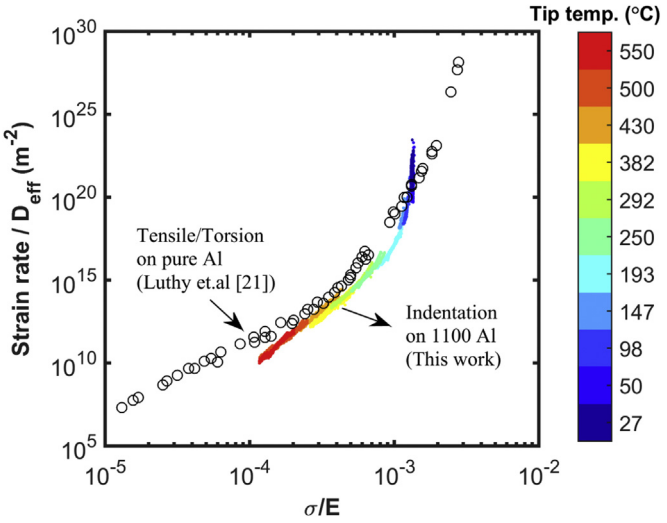

Fig. 11. Temperature compensated uniaxial strain rate as a function of normalized uniaxial stress. The plot shows the results from indentation creep experiments on 1100 Al and uniaxial tensile/torsion experiments on pure Al [21].

temperatures, it is also possible to explore the power law breakdown at higher stresses. Fig. 12 shows a Garofalo [26] type hyperbolic sine fit to the indentation creep data. The hyperbolic sine equation used is

$$\frac{\dot{\varepsilon}}{D_{eff}} = K[\sinh(a\sigma/E)]^d. \tag{10}$$

The indentation creep data fits the hyperbolic sine function well over 10 orders of magnitude, about half of which is in the power law breakdown region. As may be expected, the lower temperature region that does not correspond to effective steady state creep does not fit well. The values of a and d from the fit are 2667 and 5.4 which are close to the values (2600 and 4.8) obtained by Luthy et al. [21] for pure aluminum. In spite of the experimental challenges discussed in section 2.1, the results presented in this section clearly demonstrate the feasibility of performing high temperature indentation creep experiments over a wide range of temperatures and obtain quantitative results with a high degree of accuracy and precision.

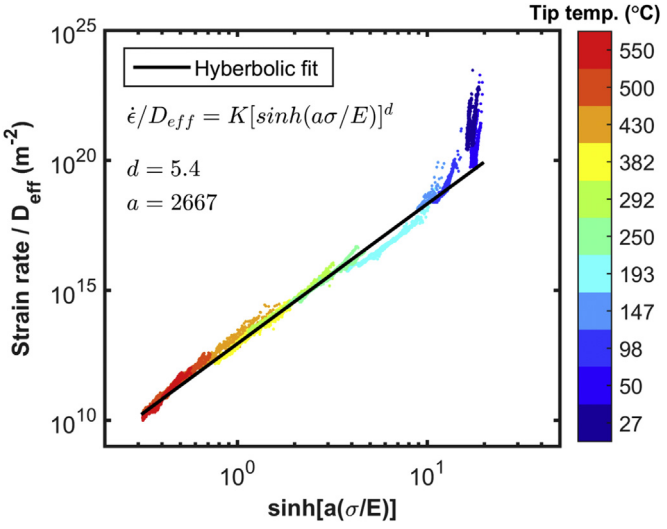

Fig. 12. Hyperbolic sine fit to the temperature compensated uniaxial strain rate and normalized uniaxial stress determined from the indentation creep tests.

4.4. Comments on the interplay of ISE, strain rate and temperature effects

In this section, we discuss the relative contributions of strain rate, temperature and ISE during indentation creep tests. While the effects of strain rate and temperature are known to be interdependent, ISE can be independent of the other two and can potentially complicate data interpretation as evident from size effect studies at different temperatures [11–13]. In order to systematically explore the relative contributions of these factors, results from constant strain rate (CSR) tests and strain rate jump tests at two different temperatures and strain rates are shown here. Fig. 13 shows the results from the CSR and strain rate jump tests at 27 °C and 400 °C. Note that these tests were performed with contact stiffness being measured continuously as a function of depth, thereby enabling hardness and modulus measurements as a function of depth. The upper portion of Fig. 13a shows the results at 27 °C and the bottom portion shows the results at 400 °C. Constant strain rate tests at 0.1 s^{-1} and 0.5 s^{-1} are shown for both the temperatures, while strain rate jump tests from 0.1 s^{-1} to 0.5 s^{-1} and vice versa are shown for 400 °C. It is evident from the plot that the test temperature has the most dominant effect on hardness

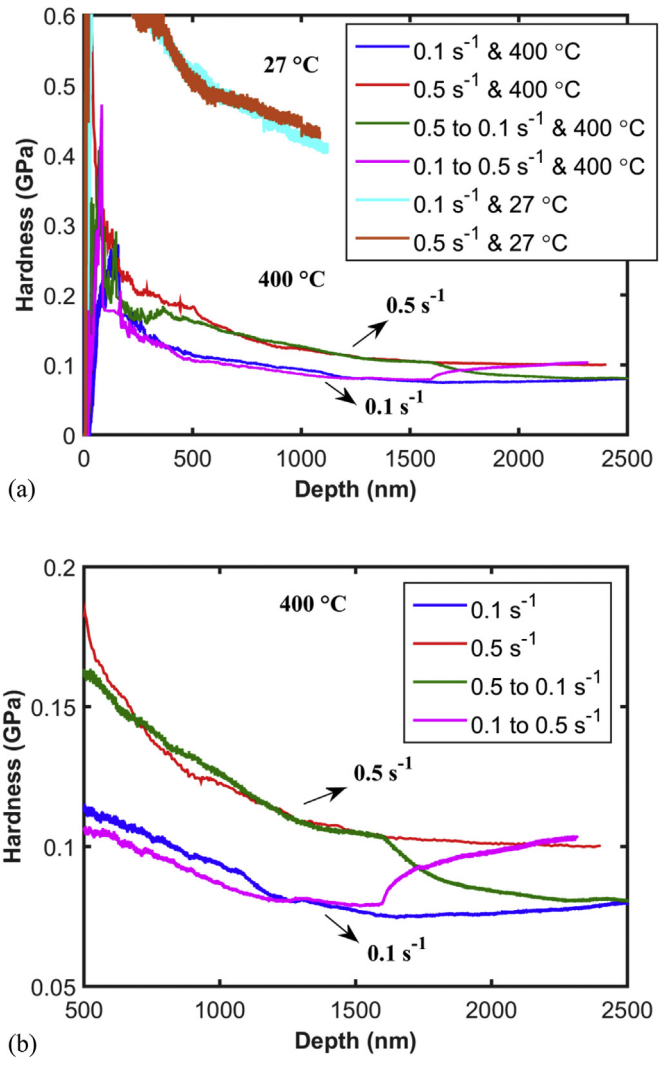

Fig. 13. Results from CSR and strain rate jump tests at (a) 27 °C and 400 °C, (b) zoomed plot of the results at 400 °C. The CSR tests are at strain rates of 0.1 s^{-1} and 0.5 s^{-1}, while the strain rate jumps are from 0.1 s^{-1} to 0.5 s^{-1} and vice versa.

wherein a significant drop in hardness can be observed at the higher temperature. For example, at a depth of 1000 nm and strain rate of 0.1 s^{-1} the hardness decreases from 0.42 GPa to 0.09 GPa with increase in temperature, which is much higher than the strain rate effect even at 400 °C. Next, the ISE can be clearly observed at all temperatures and strain rates. The size effect is more pronounced at the lower temperature as also observed in several other materials [11–13]. Franke et al. [11] have attributed this to higher mobility of defects and/or higher density of statistically stored dislocations at elevated temperatures. Also, at the lower temperature, the strain rate effect is insignificant and the ISE dominates the response. However, at 400 °C, the difference in hardness at the different strain rates is more evident and the ISE and strain rate effects are comparable. Finally, the strain rate jump tests at 400 °C from 0.1 s^{-1} to 0.5 s^{-1} and vice versa are shown in the bottom of Fig. 13a. A zoomed view of these tests is shown in Fig. 13b. It is evident from the plot that the hardness from the strain rate jump tests eventually matches the CSR tests at the corresponding strain rates even in the presence of ISE. This shows the absence of history dependence of deformation which is essential in obtaining uniaxial creep parameters from indentation using the CLH tests. In summary, these results clearly show the dominant effect of temperature on the mechanical response which is not surprising. However, the ISE can dominate the response at any given temperature and can lead to erroneous results during indentation creep testing unless proper care is taken to avoid/minimize the size effect. In this regard, CLH creep tests to large depths have a distinct advantage over strain rate jump tests.

5. Summary and conclusions

(i) High temperature nanoindentation creep tests have been performed on commercial purity aluminum (1100 Al) over a wide range of temperatures (27 °C–550 °C).
(ii) New procedures have been demonstrated for thermal drift correction and for maintaining thermal equilibrium during testing.
(iii) The activation energy for indentation creep agrees well with values determined by uniaxial experiments in similar temperature range.
(iv) Uniaxial power-law type creep constitutive behavior calculated from the indentation experiments closely matches the uniaxial results at 10% strain over a wide range of test temperatures and strain rates, demonstrating the ability to predict uniaxial creep behavior using high temperature nanoindentation. The results also show the absence of any history dependence of deformation.
(v) Indentation using a Berkovich indenter that induces a nominal strain of 8% does not result in an effective steady state indentation creep at lower temperatures (<100 °C).
(vi) The indentation creep data fits well to the hyperbolic sine function used to model power law breakdown at higher stresses.
(vii) The relative contributions of ISE, strain rate and temperature on the hardness have been explored. Temperature effects dominate the measured response while the ISE can dominate the response at any given temperature especially at lower temperatures.

Acknowledgments

The authors would like to thank Richard Anthony at Nanomechanics Inc. for help with the experimental setup.

References

[1] B.D. Beake, J.F. Smith, High-temperature nanoindentation testing of fused silica and other materials, Philos. Mag. A 82 (2002) 2179–2186, http://dx.doi.org/10.1080/01418610208235727.
[2] J.C. Trenkle, C.E. Packard, C.A. Schuh, Hot nanoindentation in inert environments, Rev. Sci. Instrum. 81 (2010) 073901, http://dx.doi.org/10.1063/1.3436633.
[3] C.A. Schuh, C.E. Packard, A.C. Lund, Nanoindentation and contact-mode imaging at high temperatures, J. Mater. Res. 21 (2011) 725–736, http://dx.doi.org/10.1557/jmr.2006.0080.
[4] N.M. Everitt, M.I. Davies, J.F. Smith, High temperature nanoindentation – the importance of isothermal contact, Philos. Mag. 91 (2011) 1221–1244, http://dx.doi.org/10.1080/14786435.2010.496745.
[5] S. Korte, R.J. Stearn, J.M. Wheeler, W.J. Clegg, High temperature microcompression and nanoindentation in vacuum, J. Mater. Res. 27 (2012) 167–176, http://dx.doi.org/10.1557/jmr.2011.268.
[6] J.M. Wheeler, P. Brodard, J. Michler, Indentation with calibrated contact temperatures, Philos. Mag. 92 (2012) 3128–3141, http://dx.doi.org/10.1080/14786435.2012.674647.
[7] J.M. Wheeler, J. Michler, Elevated temperature, nano-mechanical testing in situ in the scanning electron microscope, Rev. Sci. Instrum. 84 (2013), http://dx.doi.org/10.1063/1.4795829.
[8] C. Su, E.G. Herbert, S. Sohn, J.A. LaManna, W.C. Oliver, G.M. Pharr, Measurement of power-law creep parameters by instrumented indentation methods, J. Mech. Phys. Solids 61 (2013) 517–536, http://dx.doi.org/10.1016/j.jmps.2012.09.009.
[9] S.A. Syed Asif, J.B. Pethica, Nanoindentation creep of single-crystal tungsten and gallium arsenide, Philos. Mag. A 76 (1997) 1105–1118, http://dx.doi.org/10.1080/01418619708214217.
[10] A.F. Bower, N.A. Fleck, A. Needleman, N. Ogbonna, Indentation of a power law creeping solid, Proc. R. Soc. Lond. A Math. Phys. Eng. Sci. 441 (1993) 97–124. http://rspa.royalsocietypublishing.org/content/441/1911/97.abstract.
[11] O. Franke, J.C. Trenkle, C.A. Schuh, Temperature dependence of the indentation size effect, J. Mater. Res. 25 (2010) 1225–1229, http://dx.doi.org/10.1557/JMR.2010.0159.
[12] X. Kong, F. Sun, M. Yang, The indentation size effect in SnAgCu lead-free BGA solder joints at elevated temperatures, Electron. Packag. Technol. (2015) 1207–1210, http://dx.doi.org/10.1109/ICEPT.2015.7236796 (ICEPT), 2015 16th Int. Conf.
[13] S.-W. Lee, L. Meza, J.R. Greer, Cryogenic nanoindentation size effect in [0 0 1]-oriented face-centered cubic and body-centered cubic single crystals, Appl. Phys. Lett. 103 (2013) 101906, http://dx.doi.org/10.1063/1.4820585.
[14] H. Li, A.H.W. Ngan, Size effects of nanoindentation creep, J. Mater. Res. 19 (2004) 513–522, http://dx.doi.org/10.1557/jmr.2004.19.2.513.
[15] N. Li, L. Liu, K.C. Chan, Q. Chen, J. Pan, Deformation behavior and indentation size effect of Au49Ag5.5Pd2.3Cu26.9Si16.3 bulk metallic glass at elevated temperatures, Intermetallics 17 (2009) 227–230, http://dx.doi.org/10.1016/j.intermet.2008.07.018.
[16] G.M. Pharr, E.G. Herbert, Y. Gao, The indentation size effect: a critical examination of experimental observations and mechanistic interpretations, Annu. Rev. Mater. Res. 40 (2010) 271–292, http://dx.doi.org/10.1146/annurev-matsci-070909-104456.
[17] V. Raman, R. Berriche, An investigation of the creep processes in tin and aluminum using a depth-sensing indentation technique, J. Mater. Res. 7 (2011) 627–638, http://dx.doi.org/10.1557/JMR.1992.0627.
[18] M.J. Mayo, W.D. Nix, A micro-indentation study of superplasticity in Pb, Sn, and Sn-38 wt% Pb, Acta Metall. 36 (1988) 2183–2192.
[19] B. Lucas, An Experimental Investigation of Creep and Viscoelastic Properties Using Depth-sensing Indentation Techniques, University of Tennessee, 1997. http://trace.tennessee.edu/utk_graddiss/1255/.
[20] V. Maier, K. Durst, J. Mueller, B. Backes, H.W. Höppel, M. Göken, Nanoindentation strain-rate jump tests for determining the local strain-rate sensitivity in nanocrystalline Ni and ultrafine-grained Al, J. Mater. Res. 26 (2011) 1421–1430, http://dx.doi.org/10.1557/jmr.2011.156.
[21] H. Luthy, A.K. Miller, O.D. Sherby, The stress and temperature dependence of steady-state flow at intermediate temperatures for pure polycrystalline aluminum, Acta Metall. 28 (1980) 169–178, http://dx.doi.org/10.1016/0001-6160(80)90066-8.
[22] O.D. Sherby, R.H. Klundt, A.K. Miller, Flow stress, subgrain size, and subgrain stability at elevated temperature, Metall. Trans. A 8 (1977) 843–850, http://dx.doi.org/10.1007/BF02661565.
[23] T. Altan, F.W. Boulger, Flow stress of metals and its application in metal forming analyses, J. Eng. Ind. 95 (1973) 1009, http://dx.doi.org/10.1115/1.3438245.
[24] W.D. Nix, J.C. Gibeling, Mechanisms of time-dependent flow and fracture of metals, Flow. Fract. Elev. Temp. (1983) 1–63.
[25] D. Tabor, The Hardness of Metals, ClarendonP, 1951. https://books.google.com/books/about/The_Hardness_of_Metals.html?id=jsLRAAAAMAAJ&pgis=1 (accessed 17.06.15).
[26] F. Garofalo, An empirical relation defining the stress dependence of minimum creep rate in metals, Trans. Metall. Soc. AIME 227 (1963) 351.